

# MTI-Net: Multi-Scale Task Interaction Networks for Multi-Task Learning

Simon Vandenhende<sup>1</sup>

Stamatios Georgoulis<sup>2</sup>

Luc Van Gool<sup>1,2</sup>

<sup>1</sup>ESAT-PSI / KU Leuven    <sup>2</sup>CVL / ETH Zurich

{simon.vandenhende, luc.vangool}@kuleuven.be, {stamatios.georgoulis, vangool}@vision.ee.ethz.ch

## Abstract

*In this paper, we highlight the importance of considering task interactions at multiple scales when distilling task information in a multi-task learning setup. In contrast to common belief, we show that tasks with high pattern affinity at a certain scale are not guaranteed to retain this behaviour at other scales, and vice versa. We propose a novel architecture, MTI-Net, that builds upon this finding in three ways. First, it explicitly models task interactions at every scale via a multi-scale multi-modal distillation unit. Second, it propagates distilled task information from lower to higher scales via a feature propagation module. Third, it aggregates the refined task features from all scales via a feature aggregation unit to produce the final per-task predictions.*

*Extensive experiments on two multi-task dense labeling datasets show that, unlike prior work, our multi-task model delivers on the full potential of multi-task learning, that is, smaller memory footprint, reduced number of calculations, and better performance w.r.t. single-task learning.*

## 1. Introduction and prior work

The world around us is flooded with complex problems that require solving a multitude of tasks concurrently. An autonomous car should be able to detect all objects in the scene, localize them, understand what they are, estimate their distance and trajectory, etc. in order to safely navigate itself in its surroundings. In a similar vein, an intelligent advertisement system should be able to detect the presence of people in its viewpoint, understand their gender and age group, analyze their appearance, track where they are looking at, etc. in order to provide personalized content tied to their preferences. The examples are countless. Understandably, this calls for efficient computational models in which multiple learning tasks can be solved simultaneously.

Multi-task learning (MTL) [2, 38] tackles this problem by exploiting commonalities and differences across tasks. Compared to the single-task case, where each individual task is solved separately by its own network, multi-task

networks theoretically bring several advantages to the table. First, due to their inherent layer sharing by design, the resulting memory footprint is substantially reduced. Second, as they explicitly avoid to repeatedly calculate the features in the shared layers, once for every task, they show increased inference speeds. Most importantly, they have the potential for improved performance if the associated tasks share complementary information, or act as a regularizer for one another. Evidence for the former has been provided in the literature for certain pairs of tasks, e.g. detection and classification [10, 35], detection and segmentation [7, 13], segmentation and depth estimation [8, 48], while for the latter recent efforts point to that direction [43].

Motivated by these observations, researchers started designing architectures capable of learning shared representations from multi-task supervisory signals. Misra *et al.* [32] proposed to use "cross-stitch" units to combine features from multiple networks in order to learn a better combination of shared- and task-specific representations. Kokkinos [20] introduced an architecture called UberNet that jointly handles as many as seven tasks in a unified framework which can be trained end-to-end. Doersch and Zisserman [6] exploited multiple self-supervised tasks in order to train a single visual representation via a "lasso" regularization scheme. Zamir *et al.* [50] proposed to model the structure of space of visual tasks via finding transfer learning dependencies across a dictionary of twenty six tasks. Despite the progress reported by these or similar works [40, 28, 33, 26, 45], the joint learning of multiple tasks can lead to single-task performance degradation if information sharing happens between unrelated tasks. The latter is known as *negative transfer* [53], and has been well documented in [20] where improvement in estimating normals lead to decline in object detection, or in [13] where the multi-task version underperforms the single-task one.

To remedy this situation, a group of methods proposed to carefully balance the losses of the individual tasks, in an attempt to find an equilibrium where no task declines significantly. For example, Kendall *et al.* [17] used the homoscedastic uncertainty of each individual task to re-weight

the losses. Gradient normalization [5] was proposed to balance the losses by adaptively normalizing the magnitude of each task’s gradients. Similarly, Sinha *et al.* [42] tried to balance the losses by adapting the gradients magnitude, but differently, they employed adversarial training to this end. Dynamic task prioritization [11] proposed to dynamically sort the order of task learning, and prioritized ‘difficult’ tasks over ‘easy’ ones. Zhao *et al.* [53] introduced a modulation module to encourage feature sharing among ‘relevant’ tasks and disentangle the learning of ‘irrelevant’ tasks. Sener and Koltun [39] proposed to cast multi-task learning into a multi-objective optimization scheme, where the weighting of the different losses is adaptively changed such that a Pareto optimal solution is achieved.

In a different vein, Maninis *et al.* [30] followed a ‘single-tasking’ route. That is, in a multi-tasking framework they performed separate forward passes, one for each task, that activate shared responses among all tasks, plus some residual responses that are task-specific. Furthermore, to suppress the negative transfer issue they applied adversarial training on the gradients level that enforces them to be statistically indistinguishable across tasks.

Note that, all aforementioned works so far follow a common pattern: they *directly* predict all task outputs from the same input in one processing cycle (i.e. all predictions are generated once, in parallel or sequentially, and are not refined afterwards). By doing so, they fail to capture commonalities and differences among tasks, that are likely fruitful for one another (e.g. depth discontinuities are usually aligned with semantic edges). Arguably, this might be the reason for the moderate only performance improvements achieved by this group of works (see [30]). To alleviate this issue, a few recent works first employed a multi-task network to make initial task predictions, and then leveraged features from these initial predictions in order to further improve each task output – in an one-off or recursive manner. In particular, Xu *et al.* [48] proposed to distil information from the initial predictions of other tasks, by means of spatial attention, before adding it as a residual to the task of interest. Zhang *et al.* [51] opted for recursively predicting each task, with the intention to utilize information from past predictions of other tasks, in order to refine the features of the task of interest at each iteration. In [52], they extended upon this idea. They used a recursive procedure to propagate similar cross-task and task-specific patterns found in the initial task predictions. To do so, they operated on the affinity matrices of the initial predictions, and not on the features themselves, as was the case before.

Although better performance improvements have been reported in these works, albeit at specific datasets (see [48]), they are all based on the principle that the interactions between tasks, which are essential in the distillation or propagation procedures described above, only happen at a fixed,

local or global, scale<sup>1</sup>. For all we know, however, this is not always the case. In fact, two tasks with high pattern affinity at a certain scale are not guaranteed to retain this behaviour at other scales, and vice versa. Take for example the tasks of semantic segmentation and depth estimation, and consider the case where two cars at different distances are in front of our camera’s viewpoint, with one partially occluding the other. Looking at the local scale (i.e. patch level), the discontinuity in depth labels in the region in-between cars suggests that a similar pattern should be present in the semantic labels, i.e. there should be a change of semantic labels in the exact same region, despite the fact that this is incorrect. However, looking at the global scale this ambiguity can be resolved. An analogous observation can be made if we swapped the order of tasks, and went from global to local scale. We conclude that pattern affinities should not be considered at the task level only, as existing works do [48, 51, 52], but be conditioned on the scale level too (for a more detailed discussion visit Sec. 2.2).

In this paper, we go beyond these limitations and explicitly consider interactions at separate scales when propagating features across tasks. We propose a novel architecture, MTI-Net, that builds upon this idea. Starting from a multi-scale feature representation of the input image, generated from an off-the-shelf backbone network (e.g. [24, 46]), we make an initial prediction for each task at each considered scale. Next, for each task we distill information from other tasks by means of spatial attention to refine the features of the initial predictions. Note that, this process happens at each scale separately in order to capture the unique task interactions that happen at each individual scale, as discussed above. To tackle the limited field-of-view at higher scales, which can hinder task predictions at these scales, we propose to propagate distilled task information from the lower scales. At the final stage, the multi-scale refined features of each task are aggregated to arrive at the final predictions.

Our contributions are threefold: (1) we propose to explicitly consider multi-scale interactions when distilling information across tasks; (2) we introduce an architecture, MTI-Net, that builds upon this idea with dedicated modules, i.e. multi-scale multi-modal distillation (Sec. 2.1), feature propagation across scales (Sec. 2.4), and feature aggregation (Sec. 2.5); (3) we overcome a common obstacle of performance degradation in multi-task networks, and observe that tasks can mutually benefit each other, resulting in significant improvements w.r.t their single-task counterparts.

<sup>1</sup>With the exception of [51], where a first attempt for multi-scale processing happens at the decoding stage, in a strict sequential manner, and only for a pair of tasks, without obvious extension to multi-task learning.

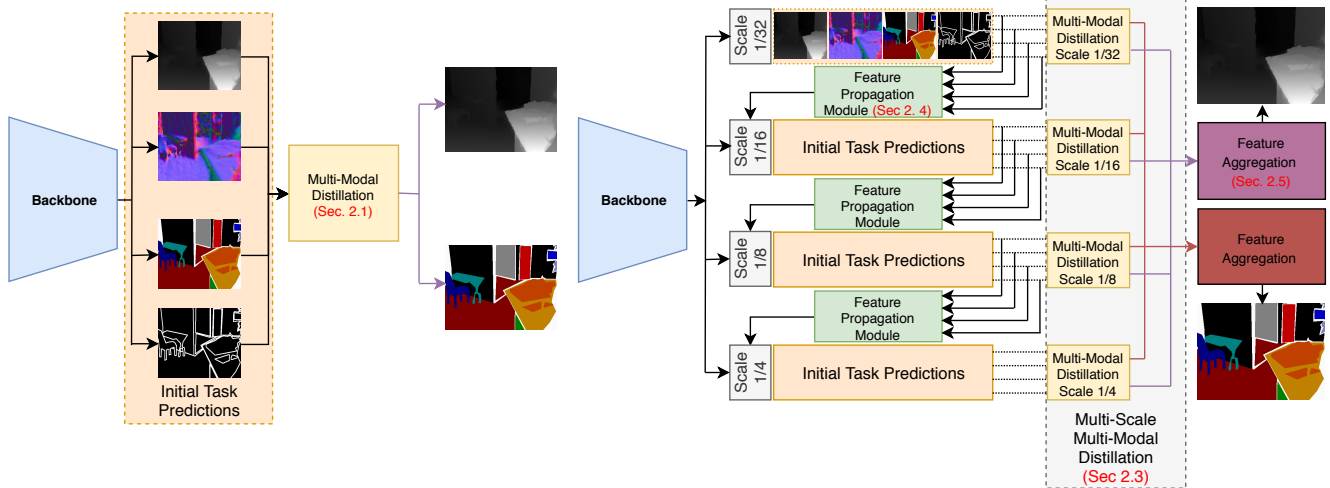


Figure 1: An overview of different MTL architectures as described in Section 2. (Left) The architecture used in PAD-Net [48] and PAP-Net [52]. Features extracted from a backbone network are used to make initial per-task predictions. The task features are combined through a distillation unit before making the final predictions. (Right) MTI-Net: Starting from a backbone that extracts multi-scale features, initial per-task predictions are made at each scale. The task features are distilled at every scale, allowing our model to capture task interactions at multiple scales, i.e. receptive fields. After distillation, the multi-scale task features are aggregated to make the final per-task predictions. To boost performance, we extend our model with a feature propagation mechanism that passes distilled information from lower resolution feature maps to higher ones.

## 2. Method

### 2.1. Multi-task learning by multi-modal distillation

Visual tasks can have relationships. For example, they can share complementary information (surface normals and depth can directly be derived from each other), act as a regularizer for one another (using RGB-D images to predict scene semantics [12] improves the quality of the prediction due to the available depth information), and so on. Motivated by this observation, recent MTL methods [48, 51, 52] have tried to explicitly distill information from other tasks, as a complementary signal in order to improve performance. Typically, this is achieved by combining an existing backbone network, that makes initial per-task predictions, with a multi-step decoding process (see Figure 1 (left)).

In more detail, the shared features of the backbone network are processed by a set of task-specific layers, that produce an initial prediction for every task. This results in a per-task feature representation of the scene that is more task-aware than the shared features of the backbone network. The information from these task-specific feature representations is then combined via a multi-modal distillation unit, before making the final task predictions. As shown in Figure 1, it is possible that some tasks are only predicted in the front-end of the network, i.e. backbone network. The latter are known as auxiliary tasks, since they serve as proxies in order to improve the performance on the final tasks.

Prior works only differ in the way that the task-specific

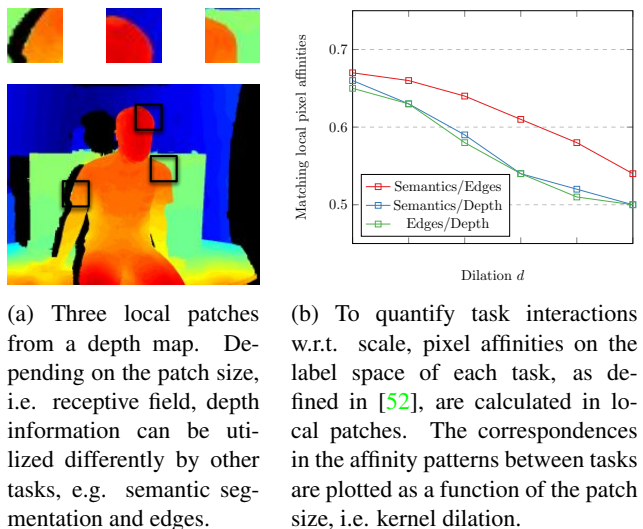


Figure 2: Unlike the common belief, we question whether task interactions remain constant across scales in Sec. 2.2.

feature representations are combined. PAD-Net [48] distills the information from other tasks by applying spatial attention before adding the features as a residual. PAP-Net [52] combines the pixel affinities from the task-specific feature representations in the final decoding step. Zhang *et al.* [51] recursively predict the tasks in order to refine the result of one task based on past experiences from another task.

## 2.2. Task interactions at different scales

The approaches described in Section 2.1 follow a common pattern: they perform multi-modal distillation at a fixed scale, i.e. the features of the backbone’s last layer. This rests on the assumption that all relevant task interactions can solely be modeled through a single filter operation with specific receptive field. For all we know, however, this is not always the case. In fact, tasks can influence each other differently at different receptive fields. Consider, for example, Figure 2a. The local patches in the depth map provide little information about the semantics of the scene. However, when we enlarge the receptive field, the depth map reveals that we are looking at an image of a person. Note that, the local patches can still provide valuable information, e.g. to improve the local alignment of edges between tasks.

To quantify the degree to which tasks share a common local structure w.r.t. the size of the receptive field, we conduct the following experiment. Inspired by [52], the pixel affinity on the label space of each task is measured in local patches, using kernels of fixed size. The size of the receptive field can be selected by choosing the dilation for the kernel. We consider the tasks of semantic segmentation, depth estimation and edge detection on the NYUD-v2 dataset. A pair of semantic pixels is similar when both pixels belong to the same category. For the depth estimation task, we threshold the relative difference between pairs of pixels. Once the pixel affinities are calculated for every task, we measure how well similar and dissimilar pairs are matched across tasks. We repeat this experiment using different dilations for the kernel, effectively changing the receptive field. The results are illustrated in Figure 2b.

A first observation is that affinity patterns are matched well across tasks, with up to 65% of pair correspondence in some cases. This indicates that different tasks can share a common structure in parts of the image. This is in agreement with a similar observation made earlier by [52].

A second observation is that the degree to which the affinity patterns are matched across tasks is dependent on the receptive field, which, in turn, corresponds to the used dilation. This validates our initial assumption that the statistic of task interactions does not always remain constant, but rather depends on the scale, i.e. receptive field.

Based on these findings, in the next section we introduce a model that distills information from different tasks at multiple scales. By doing so, we are able to capture the unique task interactions at each individual scale, overcoming the limitations of the models described in Section 2.1.

## 2.3. Multi-scale multi-modal distillation

We propose a multi-task architecture that explicitly takes into account task interactions at multiple scales. Our model is illustrated on the right side of Figure 1. First, an off-the-shelf backbone network extracts a multi-scale feature

representation from the input image. Such multi-scale feature extractors have been used in semantic segmentation [36, 46, 18], object detection [24, 46], pose estimation [34, 44], etc. In Section 3 we verify our approach using two such backbones, i.e. HRNet [46] and FPN [24], however any multi-scale feature extractor can be used instead.

From the multi-scale feature representation we make an initial prediction for every task at each scale. The task predictions at a particular scale are found by applying a set of task-specific layers to the backbone features extracted at that scale. This is similar to what [48, 52] do to get the initial task predictions from their single-scale backbone features. In our case, the result is a per-task representation of the scene at multiple scales. Not only does this add deep supervision to the network, but the per-task representations can now be distilled at each scale separately. This allows us to have multiple task interactions, each modeled within a specific receptive field, as proposed in Section 2.2.

Similar to PAD-Net [48] and PAP-Net [52], we refine each task’s features by distilling information from other tasks. Differently, we perform the multi-modal distillation at multiple scales. We use a spatial attention mechanism to fuse each task’s features with information from other tasks. The output features  $F_{k,s}^o$  for task  $k$  at scale  $s$  are found as

$$F_{k,s}^o = F_{k,s}^i + \sum_{l \neq k} \sigma(W_{k,l,s} F_{l,s}^i) \odot (W'_{k,l,s} F_{l,s}^i), \quad (1)$$

where  $\sigma(W_{k,l,s} F_{l,s}^i)$  returns a spatial attention mask that is applied to the features  $F_{l,s}^i$  from task  $l$  at scale  $s$ . Note that, our approach is not necessarily limited to the use of spatial attention, but any type of feature distillation can easily be plugged in. Through repetition, we calculate a refined feature representation for every task at every scale. As the bulk of filter operations is performed on low resolution feature maps, the computational overhead of our model is limited. We make a detailed resource analysis in Section 3.

## 2.4. Feature propagation across scales

In Section 2.3 actions at different scales were performed in isolation. As explained, we made an initial prediction for each task at every scale, from which we refined each task’s features through multi-modal distillation at each individual scale separately. However, as the higher resolution scales have a limited receptive field, the backbone network could have a hard time to make a good initial estimate of each task’s output, which, in turn, would lead to low quality task features at these scales. To remedy this situation we introduce a feature propagation mechanism, where the backbone features of a higher resolution scale are concatenated with the task features from the preceding lower resolution scale, before feeding them to the task-specific layers of the higher resolution scale to get the task features.



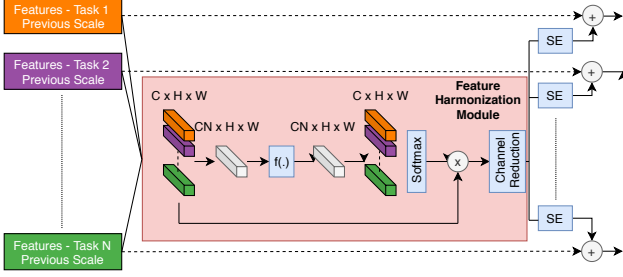


Figure 3: **Feature Propagation Module:** First, task features from a lower scale are concatenated and mapped to a shared representation by the feature harmonization module. The task features are then refined by extracting information from the shared representation through a squeeze-and-excitation (SE) block [15], and are added as a residual to the original ones. Finally, these refined task features will be concatenated with the backbone features of the preceding higher scale.

A trivial implementation for our Feature Propagation Module (FPM) would be to just upsample the task features from the previous scale and pass them to the next scale. We opt for a different approach however, and design the FPM to behave similarly to the multi-modal distillation unit of Section 2.3, in order to model task interactions at this stage too. Figure 3 gives an overview of the FPM. We first use a feature harmonization block to combine the task features from the previous scale to a shared representation. We then use this shared representation to refine the task features from the previous scale, before passing them to the next scale. The refinement happens by selecting relevant information from the shared representation through a squeeze-and-excitation block [15]. Note that, since we refine the features from a single shared representation, instead of processing each task independently as done in the multi-modal distillation unit of Section 2.3, the computational cost is significantly smaller.

**Feature harmonization** The FPM receives as input the features from  $N$  tasks of shape  $C \times H \times W$ . Our feature harmonization module combines the received features to a shared representation. The set of  $N$  task features is first concatenated and processed by a learnable non-linear function  $f$ . The output is split into  $N$  chunks along the channel dimension, that match the original number of channels  $C$ . We then apply a softmax function along the task dimension to generate a task attention mask. This is similar to the task balancing module used in [51], but we extend it here to support multiple tasks. The balanced features are concatenated and further processed to reduce the number of channels from  $N \cdot C$  to  $C$ . The output is a shared image representation based on information from all tasks.

**Refinement through Squeeze-And-Excitation** The use of a shared representation can degrade performance when

Table 1: Our multi-task learning benchmarks. We predict five tasks on PASCAL. On NYUD-v2 we only consider semantic segmentation and depth, but include edges and normals as auxiliary tasks. Distilled labels are marked with \*.

Dataset	Edge	Seg	Parts	Normals	Saliency	Depth
PASCAL	✓	✓	✓	✓*	✓*	
NYUD	✓	✓		✓		✓

tasks are unrelated. We resolve this situation by applying a per-task channel gating function to the shared representation. This effectively allows each task to select the relevant features from the shared representation. The channel gating mechanism is implemented as a squeeze-and-excitation block (SE) [15]. Note that, [30] already proposed the use of channel gating via SE when using a shared backbone to solve multiple tasks. We reuse it here in a slightly different context to extract information from the shared representation in order to refine the individual task features. After applying the SE module, the refined task features are added as a residual to the original task features.

## 2.5. Feature aggregation

The multi-scale multi-modal distillation described in Section 2.3 results in a refined per-task representation at every scale. These refined multi-scale features are upsampled to the highest scale and concatenated, resulting in a final feature representation for every task. The final task predictions are found by decoding these final feature representations in a task-specific manner again. All implementation details are discussed in Section 3. It is worth mentioning that our model has the possibility to add auxiliary tasks in the front-end, similar to PAD-Net [48]. In our case, however, the auxiliary tasks are predicted at multiple scales.

## 3. Experiments

**Datasets** We perform our experimental evaluation on two multi-task datasets. We focus on PASCAL [9], but report additional results on the smaller NYUD-v2 [41] dataset for indoor scene understanding. Table 1 contains the tasks that we considered for each dataset. We use the original 795 train and 654 test images on the NYUD-v2 dataset. On PASCAL, we use the split from PASCAL-Context [4] which has annotations for semantic segmentation, human part segmentation and edge detection. We obtain the surface normals and saliency labels from [30], that distilled them from pre-trained state-of-the-art models [1, 3].

**Implementation details** We use an FPN [24] and an HRNet [44] as our backbone networks. For HRNet, we use bilinear upsampling and concatenation followed by two convolutional layers to decode the multi-scale features. For FPN, the multi-scale features are decoded as in panoptic

feature pyramid networks [18]. All our experiments are performed with pre-trained ImageNet weights.

Our model uses two consecutive basic residual blocks [14] as task-specific layers in the front-end. When including the FPM between scales, we concatenate the backbone features of the current scale with the features that are passed from the preceding lower scale. Note that, this happens on a per-task basis, as was discussed in Section 2.4. The non-linear function that produces the task attention mask in the FPM is implemented as two basic residual blocks – that aggressively reduce the number of channels – followed by a  $1 \times 1$  convolutional layer.

We use an L1 loss for depth estimation and cross-entropy loss for semantic segmentation on NYUD-v2. As in prior work [19, 29, 30], the edge detection task is trained with a positively weighted  $w_{pos} = 0.95$  binary cross-entropy loss. We do not adopt a particular loss weighing strategy on NYUD-v2, but simply sum the losses together. On PASCAL, we reuse the exact same training setup from [30] to facilitate a fair comparison. We reuse the loss weights from there. The tasks in the front-end use the same loss weighing as the final task predictions. In contrast to [48, 52, 51], we do not use a two-step training procedure where the front-end is pretrained first. Instead, we simply train the complete architecture end-to-end. We refer to the supplementary material for a detailed overview of the used hyperparameters.

**Evaluation** We evaluate the performance of the backbone networks on the single tasks first. The optimal dataset F-measure (*odsF*) [31] is used to evaluate the edge detection task. The semantic segmentation, saliency estimation and human part segmentation tasks are evaluated using mean intersection over union (*mIoU*). We use the mean error (*mErr*) in the predicted angles to evaluate the surface normals. The depth estimation task is evaluated using the root mean square error (*rmse*). We measure the *multi-task learning performance*  $\Delta_m$  as in [30]. That is, the multi-task performance of model  $m$  is defined as the average per-task drop in performance w.r.t. the single-task baseline  $b$ :

$$\Delta_m = \frac{1}{T} \sum_{i=1}^T (-1)^{l_i} (M_{m,i} - M_{b,i}) / M_{b,i}, \quad (2)$$

where  $l_i = 1$  if a lower value means better for performance measure  $M_i$  of task  $i$ , and 0 otherwise. The single task performance is measured for a model with the same backbone.

**Performance analysis on PASCAL** We test our method on PASCAL using an HRNet18-V2 backbone. The results are reported in Table 2a. We first train a set of single-task networks. For the multi-task learning setup we discriminate between a *small set* (*s*) and *complete set* (*a*) of tasks. The small set contains the high-level (semantic and human parts segmentation) and mid-level (saliency) vision tasks. The complete set also adds the low-level (edges and normals) vision tasks. The multi-task baseline (MTL) uses a

Table 2: Multi-task learning on PASCAL.

(a) Results with an HRNet18-V2 backbone.

Method	Seg $\uparrow$	Parts $\uparrow$	Sal $\uparrow$	Edge $\uparrow$	Norm $\downarrow$	$\Delta_m \uparrow$
Single task	60.07	60.74	67.18	69.70	14.59	+ 0.00
MTL (s)	54.53	59.54	65.60	-	-	- 4.26
MTL (a)	53.60	58.45	65.13	70.60	15.08	- 3.70
Ours (s)	64.06	62.39	68.09	-	-	+ 3.35
Ours (a)	64.27	62.06	68.00	73.40	14.75	+ 2.74

(b) Results with an FPN backbone based on ResNet-18.

Method	Seg $\uparrow$	Parts $\uparrow$	Sal $\uparrow$	Edge $\uparrow$	Norm $\downarrow$	$\Delta_m \uparrow$
Single task	64.49	57.43	66.38	68.20	14.77	+ 0.00
MTL (s)	54.51	55.12	64.76	-	-	- 7.32
MTL (a)	59.61	56.88	64.96	70.60	15.17	- 1.80
Ours (s)	65.47	61.32	66.37	-	-	+ 2.77
Ours (a)	65.69	61.59	66.76	73.90	14.55	+ 3.84

(c) Results with an FPN backbone based on ResNet-50.

Method	Seg $\uparrow$	Parts $\uparrow$	Sal $\uparrow$	Edge $\uparrow$	Norm $\downarrow$	$\Delta_m \uparrow$
Single task	67.71	61.83	67.18	71.11	14.76	+ 0.00
MTL (s)	60.34	59.66	64.98	-	-	- 5.49
MTL (a)	60.63	58.72	65.10	70.60	15.46	- 4.55
Ours (s)	68.03	64.37	67.28	-	-	+ 1.53
Ours (a)	66.56	63.31	66.61	74.90	14.55	+ 1.36

set of task-specific convolutional layers to decode the backbone features. The MTL baseline leads to decreased performance,  $-4.26\%$  and  $-3.70\%$  on the small and complete set respectively. This is inline with prior work [45, 30].

Our model improves over a set of single-task models ( $+3.35\%$ ) on the small task set (*s*). We obtain solid improvements on all tasks. We do not report the influence of adding additional auxiliary tasks here, i.e. normals and edges, but we provide these results on the supplementary material. The numbers reported there show that the use of auxiliary tasks can usually further improve the results.

We also consider jointly solving all five tasks together. Again, our model outperforms ( $+2.74\%$ ) the set of single task models. All tasks gain significantly, except for normals where we see a small decrease in performance (less than one degree). We refer to Figure 5 for qualitative results.

We include additional results when using an FPN with ResNet18 and ResNet50 backbone in Tab. 6b and 7b respectively. Again, the multi-task performance of our model is positive. We observe that our method is not tied to a specific backbone network. To the best of our knowledge, we are the first to report solid improvements over the single task models, when jointly predicting such diverse set of tasks.

Finally, we compare our results to the state-of-the-art in Table 3. We include the performance of the single-task (ST) and multi-task (MT) models for different backbones. We also include the multi-task performance relative to the corresponding single-task models ( $\Delta_m$  (ST)), as well as to the single-task ResNet-50 DeepLab-v3+ models from [30]. Our model significantly outperforms attentive single-tasking of multiple tasks (ASTMT) in terms

Table 3: Comparison with the state-of-the-art on PASCAL. The \* are meant to show that our HRNet-32 multi-task model was trained with half the batch size w.r.t. all other models due to GPU memory constraints.

Model	Backbone	Seg $\uparrow$		Parts $\uparrow$		Sal $\uparrow$		Edge $\uparrow$		Norm $\downarrow$		$\Delta_m \uparrow$ (ST)	$\Delta_m \uparrow$ (R50-DLv3+)
		ST	MT	ST	MT	ST	MT	ST	MT	ST	MT		
ASTMT [30]	R26-DeepLab-v3+	64.9	64.6	57.1	57.3	64.2	64.7	71.3	71.0	14.9	15.0	- 0.11	- 3.43
	R50-DeepLab-v3+	68.3	68.0	60.70	61.1	65.4	65.7	72.7	72.4	14.6	14.7	- 0.04	- 0.04
	R50-Uber	66.9	65.5	59.8	60.2	64.6	65.0	71.7	70.5	15.0	14.9	- 0.43	- 2.12
	R101-DeepLab-v3+	69.8	68.5	63.5	63.4	67.4	67.7	73.5	73.5	14.2	14.4	- 0.60	+ 2.15
MTI-Net (Ours)	R18-FPN	64.5	65.7	57.4	61.6	66.4	66.8	68.2	73.9	14.8	14.6	+ 3.84	+ 0.34
	R50-FPN	67.7	66.6	61.8	63.3	67.2	66.6	71.1	74.9	14.8	14.6	+ 1.36	+ 1.39
	HRNet-18	60.1	64.3	60.7	62.1	67.2	68.0	69.7	73.4	14.6	14.8	+ 2.74	+ 0.05
	HRNet-32	70.2	69.3*	66.3	67.0*	68.0	68.4*	72.7	74.9*	14.3	14.2*	+ 0.82*	+ 4.43*

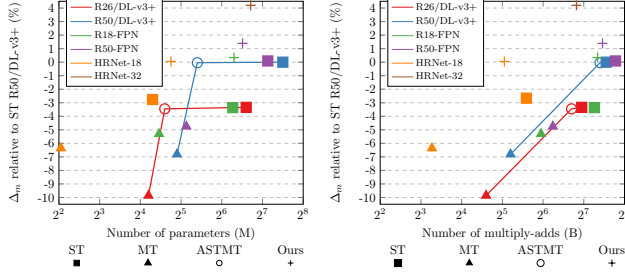


Figure 4: **Resource analysis:** We plot the multi-task learning performance  $\Delta_m$  relative to the single-task DeepLab-v3+ models with ResNet-50 backbone from [30], as a function of the number of parameters (left) and number of multiply-adds (right).

of relative improvement w.r.t. single-tasks and ResNet-50 DeepLab-v3+. Note that, ASTMT requires one forward pass per task, while we predict all tasks in a single pass.

Surprisingly, we find that our model with ResNet-18 backbone outperforms the single-tasking ResNet-50 DeepLab-v3+ models (+0.34%) in terms of multi-task performance. The individual task performance improves or remains equal except for the semantic segmentation task. We hypothesize that this is due to the amount of finetuning that went into the construction of the Deeplab-v3+ model for the semantic segmentation task (e.g. dilated convolutions, ASPP module, etc.). Another notable result is that our ResNet-18 model outperforms an UberNet [20] with ResNet-50 backbone on all tasks. Finally, when using the deeper HRNet32-V2 backbone, we even outperform the deeper ASTMT ResNet-101 DeepLab-v3+ model on all tasks. Note, how the performance w.r.t. single-tasks still increases in our case, despite using half the batch size due to GPU constraints, but decreases in their case as we move to deeper backbone networks.

**Resource analysis on PASCAL** Figure 4 plots the multi-task performance as a function of the computational requirements (number of parameters and FLOPS). We measure the latter as the average per-task performance drop compared to the single-task ResNet-50 models from [30] (blue rectangles), similarly to the last column in Table 3.

Table 4: Ablation studies on NYUD-v2 using an HRNet18-V2 backbone. Auxiliary tasks are given within brackets.

Method	Segm (IoU)	Depth (rmse)	$\Delta_m$ %
Single task	33.18	0.667	+ 0.00
MTL	32.09	0.668	- 1.71
PAD-Net	32.80	0.660	- 0.02
PAD-Net (N)	33.85	0.658	+ 1.65
PAD-Net (N+E)	32.92	0.655	+ 0.52
Ours - w/o FPM	34.38	0.640	+ 3.85
Ours - w/o FPM (N)	34.49	0.642	+ 3.84
Ours - w/o FPM (N+E)	34.68	0.637	+ 4.48
Ours - w/ FPM	35.12	0.620	+ 6.40
Ours - w/ FPM (N)	36.22	<b>0.600</b>	+ 9.57
Ours - w/ FPM (N+E)	<b>37.49</b>	0.607	<b>+ 10.91</b>

Table 5: Comparison with the state-of-the-art on NYUD-v2.

(a) Results on the depth estimation task.

Method	rmse	rel	$\delta_1$	$\delta_2$	$\delta_3$
HCRF [21]	0.821	0.232	0.621	0.886	0.968
DCNF [25]	0.824	0.230	0.614	0.883	0.971
Wang [47]	0.745	0.220	0.605	0.890	0.970
NR forest [37]	0.774	0.187	-	-	-
Xu [49]	0.593	0.125	0.806	0.952	0.986
PAD-Net [48]	0.582	<b>0.120</b>	0.817	0.954	0.987
PAP-Net [52]	0.530	0.144	0.815	0.962	0.992
ST - HRNet48-V2	0.547	0.138	0.828	0.966	0.993
Ours - HRNet48-V2	<b>0.529</b>	0.138	<b>0.830</b>	<b>0.969</b>	<b>0.993</b>

(b) Results on the semantic segmentation task.

Method	pixel-acc	mean-acc	IoU
FCN [27]	60.0	49.2	29.2
Context [23]	70.0	53.6	40.6
Eigen [8]	65.6	45.1	34.1
B-SegNet [16]	68.0	45.8	32.4
RefineNet-101 [22]	72.8	57.8	44.9
PAD-Net [48]	75.2	62.3	50.2
TRL-ResNet50 [51]	76.2	56.3	46.4
PAP-Net [52]	<b>76.2</b>	62.5	<b>50.4</b>
ST - HRNet48-V2	73.4	58.1	45.7
Ours - HRNet48-V2	75.3	<b>62.9</b>	49.0

The multi-task baseline models (triangle) decrease the performance, but require less parameters and FLOPS. The ASTMT model (circle) performs on par with the single-task models, while using much less parameters. However, our models achieve the best performance for any given computational budget, be it number of parameters or FLOPS.

**Ablation studies on NYUD-v2** Table 4 reports additional results on the smaller NYUD-v2 dataset to verify how



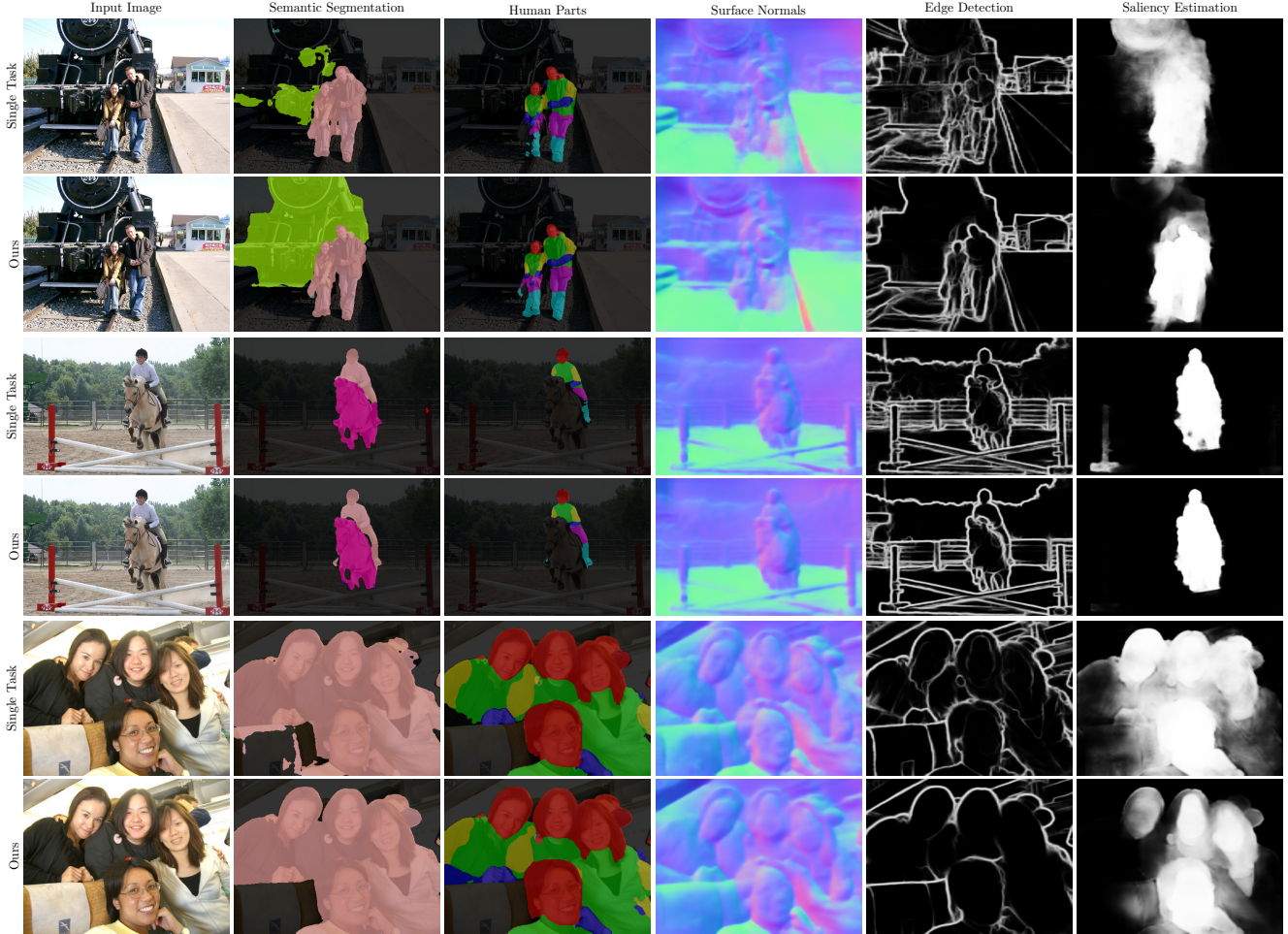


Figure 5: **Qualitative results on PASCAL.** We compare the predictions made by a set of single task models (first row for every image) against the predictions made by our MTI-Net (second row for every image). Differences can be seen for semantic segmentation, edge detection and saliency estimation. We used an HRNet18-V2 model as backbone.

different parts of the model contribute to the multi-task improvements. We use an HRNet18-V2 backbone. Our main tasks are semantic segmentation and depth prediction. Edge detection and surface normals prediction are considered as auxiliary tasks. The supplementary materials contain additional results for an FPN with ResNet-18 backbone.

As before, the MTL baseline with shared encoder has lower performance ( $-1.71\%$ ) than the single-task models. As reported in [48], PAD-Net improves over the single task models. Using our model without the FPM between scales further improves the results ( $+3.85\%$ ). Finally, we also include the FPM which is responsible for another significant boost in performance ( $+6.40\%$ ). Adding the surface normals and edges as auxiliary tasks can help to improve the quality of the predictions. This is especially the case when including the FPM into our model ( $+9.57\%$  and  $+10.91\%$ ).

Finally, we perform a comparison with the state-of-the-

art on NYUD-v2 in Table 5. We do not consider methods that rely on extra input modalities, or additional training data. We use a deeper HRNet48-v2 backbone. Our model performs on par with the state-of-the-art on the depth estimation task, while performing slightly worse on the semantic segmentation task. Again, we find that our model improves w.r.t the single-task models. We refer the reader to the supplementary materials for qualitative results.

## 4. Conclusion

We have shown the importance of modeling task interactions at multiple scales, enabling tasks to maximally benefit each other. We achieved this by introducing dedicated modules on top of an off-the-shelf multi-scale feature extractor, i.e. multi-scale multi-modal distillation, feature propagation across scales, and feature aggregation. Our multi-task model delivers on the full potential of multi-task learning,



i.e. smaller memory footprint, reduced number of calculations and better performance. Our experiments show that our multi-task models consistently outperform their single-tasking counterparts by medium to large margins.

**Acknowledgment** The authors thankfully acknowledge support by Toyota via the TRACE project.

## References

- [1] Aayush Bansal, Xinlei Chen, Bryan Russell, Abhinav Gupta, and Deva Ramanan. Pixelnet: Representation of the pixels, by the pixels, and for the pixels. *arXiv preprint arXiv:1702.06506*, 2017. 5
- [2] Rich Caruana. Multitask learning. *Machine learning*, 28(1):41–75, 1997. 1
- [3] Liang-Chieh Chen, Yukun Zhu, George Papandreou, Florian Schroff, and Hartwig Adam. Encoder-decoder with atrous separable convolution for semantic image segmentation. In *ECCV*, pages 801–818, 2018. 5
- [4] Xianjie Chen, Roozbeh Mottaghi, Xiaobai Liu, Sanja Fidler, Raquel Urtasun, and Alan Yuille. Detect what you can: Detecting and representing objects using holistic models and body parts. In *CVPR*, pages 1971–1978, 2014. 5
- [5] Zhao Chen, Vijay Badrinarayanan, Chen-Yu Lee, and Andrew Rabinovich. Gradnorm: Gradient normalization for adaptive loss balancing in deep multitask networks. In *ICML*, 2018. 2
- [6] Carl Doersch and Andrew Zisserman. Multi-task self-supervised visual learning. In *ICCV*, pages 2051–2060, 2017. 1
- [7] Nikita Dvornik, Konstantin Shmelkov, Julien Mairal, and Cordelia Schmid. Blitznet: A real-time deep network for scene understanding. In *ICCV*, pages 4154–4162, 2017. 1
- [8] David Eigen and Rob Fergus. Predicting depth, surface normals and semantic labels with a common multi-scale convolutional architecture. In *ICCV*, pages 2650–2658, 2015. 1, 7
- [9] Mark Everingham, Luc Van Gool, Christopher KI Williams, John Winn, and Andrew Zisserman. The pascal visual object classes (voc) challenge. *IJCV*, 88(2):303–338, 2010. 5
- [10] Ross Girshick. Fast r-cnn. In *ICCV*, pages 1440–1448, 2015. 1
- [11] Michelle Guo, Albert Haque, De-An Huang, Serena Yeung, and Li Fei-Fei. Dynamic task prioritization for multitask learning. In *ECCV*, 2018. 2
- [12] Saurabh Gupta, Ross Girshick, Pablo Arbeláez, and Jitendra Malik. Learning rich features from rgb-d images for object detection and segmentation. In *ECCV*, pages 345–360. Springer, 2014. 3
- [13] Kaiming He, Georgia Gkioxari, Piotr Dollár, and Ross Girshick. Mask r-cnn. In *ICCV*, pages 2961–2969, 2017. 1
- [14] Kaiming He, Xiangyu Zhang, Shaoqing Ren, and Jian Sun. Deep residual learning for image recognition. In *CVPR*, pages 770–778, 2016. 6
- [15] Jie Hu, Li Shen, and Gang Sun. Squeeze-and-excitation networks. In *CVPR*, pages 7132–7141, 2018. 5
- [16] Alex Kendall, Vijay Badrinarayanan, and Roberto Cipolla. Bayesian segnet: Model uncertainty in deep convolutional encoder-decoder architectures for scene understanding. *arXiv preprint arXiv:1511.02680*, 2015. 7
- [17] Alex Kendall, Yarin Gal, and Roberto Cipolla. Multi-task learning using uncertainty to weigh losses for scene geometry and semantics. In *CVPR*, 2018. 1
- [18] Alexander Kirillov, Ross Girshick, Kaiming He, and Piotr Dollár. Panoptic feature pyramid networks. In *CVPR*, pages 6399–6408, 2019. 4, 6
- [19] Iasonas Kokkinos. Pushing the boundaries of boundary detection using deep learning. *arXiv preprint arXiv:1511.07386*, 2015. 6
- [20] Iasonas Kokkinos. Ubertnet: Training a universal convolutional neural network for low-, mid-, and high-level vision using diverse datasets and limited memory. In *CVPR*, 2017. 1, 7
- [21] Bo Li, Chunhua Shen, Yuchao Dai, Anton Van Den Hengel, and Mingyi He. Depth and surface normal estimation from monocular images using regression on deep features and hierarchical crfs. In *CVPR*, pages 1119–1127, 2015. 7
- [22] Guosheng Lin, Anton Milan, Chunhua Shen, and Ian Reid. Refinenet: Multi-path refinement networks for high-resolution semantic segmentation. In *CVPR*, pages 1925–1934, 2017. 7
- [23] Guosheng Lin, Chunhua Shen, Anton Van Den Hengel, and Ian Reid. Efficient piecewise training of deep structured models for semantic segmentation. In *CVPR*, pages 3194–3203, 2016. 7
- [24] Tsung-Yi Lin, Piotr Dollár, Ross Girshick, Kaiming He, Bharath Hariharan, and Serge Belongie. Feature pyramid networks for object detection. In *CVPR*, pages 2117–2125, 2017. 2, 4, 5
- [25] Fayao Liu, Chunhua Shen, Guosheng Lin, and Ian Reid. Learning depth from single monocular images using deep convolutional neural fields. *TPAMI*, 38(10):2024–2039, 2015. 7
- [26] Shikun Liu, Edward Johns, and Andrew J Davison. End-to-end multi-task learning with attention. In *CVPR*, 2019. 1
- [27] Jonathan Long, Evan Shelhamer, and Trevor Darrell. Fully convolutional networks for semantic segmentation. In *CVPR*, pages 3431–3440, 2015. 7
- [28] Yongxi Lu, Abhishek Kumar, Shuangfei Zhai, Yu Cheng, Tara Javidi, and Rogerio Feris. Fully-adaptive feature sharing in multi-task networks with applications in person attribute classification. In *CVPR*, 2017. 1
- [29] Kevis-Kokitsi Maninis, Jordi Pont-Tuset, Pablo Arbeláez, and Luc Van Gool. Convolutional oriented boundaries: From image segmentation to high-level tasks. *TPAMI*, 40(4):819–833, 2017. 6
- [30] Kevis-Kokitsi Maninis, Ilija Radosavovic, and Iasonas Kokkinos. Attentive single-tasking of multiple tasks. In *CVPR*, pages 1851–1860, 2019. 2, 5, 6, 7, 12
- [31] David R Martin, Charless C Fowlkes, and Jitendra Malik. Learning to detect natural image boundaries using local brightness, color, and texture cues. *TPAMI*, (5):530–549, 2004. 6

- [32] Ishan Misra, Abhinav Shrivastava, Abhinav Gupta, and Martial Hebert. Cross-stitch networks for multi-task learning. In *CVPR*, 2016. 1
- [33] Davy Neven, Bert De Brabandere, Stamatios Georgoulis, Marc Proesmans, and Luc Van Gool. Fast scene understanding for autonomous driving. In *IV Workshops*, 2017. 1
- [34] Alejandro Newell, Kaiyu Yang, and Jia Deng. Stacked hourglass networks for human pose estimation. In *ECCV*, pages 483–499. Springer, 2016. 4
- [35] Shaoqing Ren, Kaiming He, Ross Girshick, and Jian Sun. Faster r-cnn: Towards real-time object detection with region proposal networks. In *NIPS*, pages 91–99, 2015. 1
- [36] Olaf Ronneberger, Philipp Fischer, and Thomas Brox. U-net: Convolutional networks for biomedical image segmentation. In *International Conference on Medical image computing and computer-assisted intervention*, pages 234–241. Springer, 2015. 4
- [37] Anirban Roy and Sinisa Todorovic. Monocular depth estimation using neural regression forest. In *CVPR*, pages 5506–5514, 2016. 7
- [38] Sebastian Ruder. An overview of multi-task learning in deep neural networks. *arXiv preprint arXiv:1706.05098*, 2017. 1
- [39] Ozan Sener and Vladlen Koltun. Multi-task learning as multi-objective optimization. In *NIPS*, 2018. 2
- [40] Pierre Sermanet, David Eigen, Xiang Zhang, Michaël Mathieu, Rob Fergus, and Yann LeCun. Overfeat: Integrated recognition, localization and detection using convolutional networks. *arXiv preprint arXiv:1312.6229*, 2013. 1
- [41] Nathan Silberman, Derek Hoiem, Pushmeet Kohli, and Rob Fergus. Indoor segmentation and support inference from rgb-d images. In *ECCV*, pages 746–760. Springer, 2012. 5
- [42] Ayan Sinha, Zhao Chen, Vijay Badrinarayanan, and Andrew Rabinovich. Gradient adversarial training of neural networks. *arXiv preprint arXiv:1806.08028*, 2018. 2
- [43] Trevor Standley, Amir R Zamir, Dawn Chen, Leonidas Guibas, Jitendra Malik, and Silvio Savarese. Which tasks should be learned together in multi-task learning? *arXiv preprint arXiv:1905.07553*, 2019. 1
- [44] Ke Sun, Bin Xiao, Dong Liu, and Jingdong Wang. Deep high-resolution representation learning for human pose estimation. In *CVPR*, pages 5693–5703, 2019. 4, 5
- [45] Simon Vandenhende, Stamatios Georgoulis, Bert De Brabandere, and Luc Van Gool. Branched multi-task networks: Deciding what layers to share. *arXiv preprint arXiv:1904.02920*, 2019. 1, 6
- [46] Jingdong Wang, Ke Sun, Tianheng Cheng, Borui Jiang, Chaorui Deng, Yang Zhao, Dong Liu, Yadong Mu, Mingkui Tan, Xinggang Wang, et al. Deep high-resolution representation learning for visual recognition. *arXiv preprint arXiv:1908.07919*, 2019. 2, 4
- [47] Peng Wang, Xiaohui Shen, Zhe Lin, Scott Cohen, Brian Price, and Alan L Yuille. Towards unified depth and semantic prediction from a single image. In *CVPR*, pages 2800–2809, 2015. 7
- [48] Dan Xu, Wanli Ouyang, Xiaogang Wang, and Nicu Sebe. Pad-net: Multi-tasks guided prediction-and-distillation network for simultaneous depth estimation and scene parsing. In *CVPR*, pages 675–684, 2018. 1, 2, 3, 4, 5, 6, 7, 8, 11
- [49] Dan Xu, Wei Wang, Hao Tang, Hong Liu, Nicu Sebe, and Elisa Ricci. Structured attention guided convolutional neural fields for monocular depth estimation. In *CVPR*, pages 3917–3925, 2018. 7
- [50] Amir R Zamir, Alexander Sax, William Shen, Leonidas J Guibas, Jitendra Malik, and Silvio Savarese. Taskonomy: Disentangling task transfer learning. In *CVPR*, 2018. 1
- [51] Zhenyu Zhang, Zhen Cui, Chunyan Xu, Zequn Jie, Xiang Li, and Jian Yang. Joint task-recursive learning for semantic segmentation and depth estimation. In *ECCV*, pages 235–251, 2018. 2, 3, 5, 6, 7
- [52] Zhenyu Zhang, Zhen Cui, Chunyan Xu, Yan Yan, Nicu Sebe, and Jian Yang. Pattern-affinitive propagation across depth, surface normal and semantic segmentation. In *CVPR*, pages 4106–4115, 2019. 2, 3, 4, 6, 7
- [53] Xiangyun Zhao, Haoxiang Li, Xiaohui Shen, Xiaodan Liang, and Ying Wu. A modulation module for multi-task learning with applications in image retrieval. In *ECCV*, 2018. 1, 2

## A. PASCAL

We consider the effect of including auxiliary tasks as extra supervision on the PASCAL dataset. In particular, we consider the small task set ( $s$ ) - semantic segmentation, human parts prediction and saliency detection - as our main tasks, and we measure the performance when adding edge detection and surface normals prediction as auxiliary tasks to the front-end of the network. Table 6 contains the results for two backbones. When adding edge detection as an auxiliary task, the results are further improved. However, this is not the case when we add surface normals prediction as an auxiliary task. We observe a similar effect when including both edge detection and surface normals prediction. We believe that this is due to the approximate nature of the surface normals in this dataset, as the latter were obtained through distillation, and as such they are rather noisy.

Table 6: Multi-task learning on PASCAL. We consider the effect of adding auxiliary tasks to the front-end of the network. In particular we add edge prediction (E) and surface normals estimation (N) as auxiliary tasks.

(a) Results with an HRNet18-V2 backbone.

Method	Seg $\uparrow$	Parts $\uparrow$	Sal $\uparrow$	$\Delta_m \uparrow$
Single task	60.07	60.74	67.18	+ 0.00
Ours (s)	64.06	62.39	68.09	+ 3.35
Ours (s)(E)	64.98	62.90	67.84	+ 3.98
Ours (s)(N)	63.74	61.75	67.90	+2.69
Ours (s)(E+N)	64.33	62.33	68.00	+3.36

(b) Results with an FPN backbone based on ResNet-18.

Method	Seg $\uparrow$	Parts $\uparrow$	Sal $\uparrow$	$\Delta_m \uparrow$
Single task	64.49	57.43	66.38	+ 0.00
Ours (s)	65.47	61.32	66.37	+ 2.77
Ours (s)(E)	65.93	62.21	66.80	+ 3.61
Ours (s)(N)	64.99	61.09	66.80	+ 2.52
Ours (s)(E+N)	65.46	61.71	66.62	+ 3.06

## B. NYUD-v2

This section contains additional results on the NYUD-v2 dataset. Section B.1 gives a more detailed view on the ablation studies that we performed on NYUD-v2 using an HRNet18v2 backbone. Note that the main results of this experiment were already discussed in the experiments section of the paper. In Section B.2, we perform an additional experiment using an FPN backbone based on ResNet-18.

### B.1. HRNet18-V2

Table 7 contains additional metrics for the depth estimation and semantic segmentation task on the NYUD-v2

dataset, when using an HRNet18-v2 backbone. This is an extension to the metrics shown in Table 4 of the paper.

Table 7: Ablation studies on NYUD-v2 using an HRNet18-V2 backbone. Auxiliary tasks are indicated in brackets.

(a) Results on the depth estimation task.

Method	rmse $\downarrow$	rel $\downarrow$	$\delta_1 \uparrow$	$\delta_2 \uparrow$	$\delta_3 \uparrow$
Single task	0.667	0.186	0.731	0.931	0.981
MTL	0.668	0.193	0.717	0.927	0.980
PAD-Net	0.660	0.189	0.726	0.930	0.981
PAD-Net (N)	0.658	0.187	0.726	0.932	0.982
PAD-Net (N+E)	0.655	0.184	0.731	0.934	0.982
Ours - w/o FPM	0.640	0.181	0.747	0.937	0.982
Ours - w/o FPM (N)	0.642	0.175	0.753	0.940	0.983
Ours - w/o FPM (N+E)	0.637	0.174	0.757	0.939	0.984
Ours - w/ FPM	0.620	0.161	0.781	0.946	0.986
Ours - w/ FPM (N)	0.600	0.162	0.788	0.947	0.985
Ours - w/ FPM (N+E)	0.607	0.166	0.783	0.945	0.985

(b) Results on the semantic segmentation task.

Method	pixel-acc $\uparrow$	mean-acc $\uparrow$	IoU $\uparrow$
Single task	65.04	45.07	33.18
MTL	64.61	43.55	32.09
PAD-Net	65.00	44.61	32.80
PAD-Net (N)	64.77	46.28	33.85
PAD-Net (N+E)	65.05	44.79	32.92
Ours - w/o FPM	65.52	45.98	34.38
Ours - w/o FPM (N)	65.27	46.63	34.49
Ours - w/o FPM (N+E)	66.15	46.97	34.68
Ours - w/ FPM	66.30	47.85	35.12
Ours - w/ FPM (N)	66.98	49.04	36.22
Ours - w/ FPM (N+E)	68.03	51.05	37.49

## B.2. FPN - ResNet-18

We repeated a smaller version of our ablation studies on the NYUD-v2 dataset when using an FPN backbone based on ResNet-18. Table 8 contains the results. We end up at similar findings compared to the model based on HRNet18-v2. Again, we see a significant improvement over the set of single-task models. Additionally, we find that the use of auxiliary tasks can help to improve the quality of the predictions, as the latter are not distilled in this case.

## B.3. HRNet48-V2

Figure 6 shows predictions made by our HRNet48-v2 model on images from the NYUD-v2 test set. The quantitative results were already reported in Table 5 of the paper.

## C. Training setup

Finally, we include a detailed description of the training setup used for each experiment.

### C.1. NYUD-v2

We applied the data augmentation strategy of [48]. The RGB and depth images were randomly scaled with the selected ratio in  $\{1, 1.2, 1.5\}$ , and randomly horizontally flipped. The model was trained for 80 epochs with an Adam

Table 8: Additional results on NYUD-v2 when using an FPN backbone based on ResNet-18. Similarly to Table 2, auxiliary tasks are indicated in brackets.

(a) Multi-task learning performance.

Method	Segm (IoU) $\uparrow$	Depth (rmse) $\downarrow$	$\Delta_m$ %
Single task	34.46	0.659	+0.00
MTL	33.52	0.665	-1.82
PAD-Net	34.15	0.662	-0.69
PAD-Net (N)	34.18	0.657	-0.23
PAD-Net (N+E)	34.60	0.668	-0.45
Ours	36.01	0.630	+4.43
Ours (N)	36.81	0.628	+5.74
Ours (N+E)	36.65	0.618	+6.27

(b) Results on the depth estimation task.

Method	rmse $\downarrow$	rel $\downarrow$	$\delta_1$ $\uparrow$	$\delta_2$ $\uparrow$	$\delta_3$ $\uparrow$
Single task	0.659	0.183	0.730	0.935	0.982
MTL	0.665	0.190	0.726	0.930	0.980
PAD-Net	0.662	0.188	0.731	0.931	0.979
PAD-Net (N)	0.657	0.185	0.735	0.934	0.980
PAD-Net (N+E)	0.668	0.185	0.729	0.933	0.980
Ours	0.630	0.173	0.767	0.939	0.981
Ours (N)	0.628	0.180	0.755	0.939	0.982
Ours (N+E)	0.618	0.169	0.768	0.944	0.984

(c) Results on the semantic segmentation task.

Method	pixel-acc $\uparrow$	mean-acc $\uparrow$	IoU $\uparrow$
Single task	65.51	46.50	34.46
MTL	64.85	45.33	33.52
PAD-Net	65.23	45.65	34.15
PAD-Net (N)	65.07	45.80	34.18
PAD-Net (N+E)	65.68	46.77	34.60
Ours	66.44	49.03	36.01
Ours (N)	66.89	50.50	36.81
Ours (N+E)	67.23	49.93	36.65

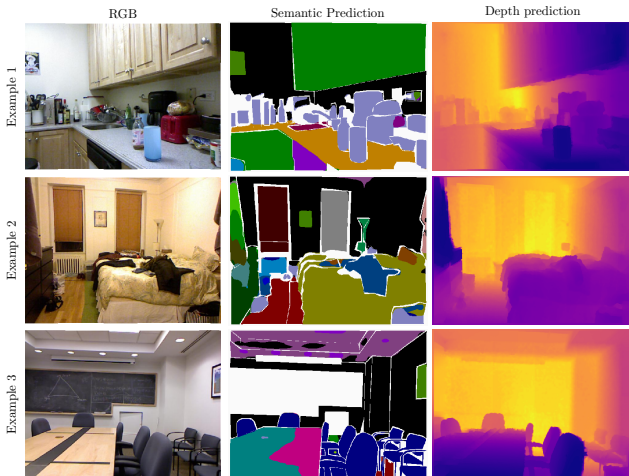


Figure 6: **Qualitative results on NYUD-v2:** Semantic and depth predictions made by our HRNet48-V2 model.

optimizer with initial learning rate  $1e-4$  and batches of size 6. We used a poly learning rate decay scheme. All experiments used pre-trained weights from ImageNet.

## C.2. PASCAL

We essentially plugged our model into the code base that was shared by [30]. In particular, the single-task models were trained with stochastic gradient descent with momentum 0.9. We used batches of size 8 and a poly learning rate decay scheme. The initial learning rate was 0.01. We applied weight decay  $\lambda = 1e-4$ . These hyperparameters are the same as the ones used in [30], ensuring fair comparison. The multi-task baseline models were trained using the same hyperparameters. The multi-task loss weighing was taken from [30]. We also tested the use of an Adam optimizer, but this did not yield better results.

Our MTI-Net was trained under the same settings as the single-task models, but we used an Adam optimizer with initial learning rate  $1e-4$ . We re-used the loss weights from before to weight the losses from the initial task predictions.